Table S1: Pathway and assay selection.

Category	Criteria
Relevant, included in manuscript	1. Function can be assessed by visualization of morphology. 2. Essential cellular pathway involved in a broad array of cellular functions. 3. Altered morphology of the cellular compartment is associated with pathophysiology of disease(s). 4. Reliable markers exist that aid visualization.
Relevant, but not included in manuscript	1. Assay meets al criteria of relevance, but has not yet been included for this project.
Assay does not meet criteria of relevance	1. Function cannot be assessed by visualizing morphology. 2. Highly specific cellular pathway or only involved in a small subset of cellular functions. 3. Altered morphology of the cellular compartment is not associated with disease. 4. Reliable markers for the pathway do not exist

Cellular component	Function	Marker	Diseases associated with dysfunction	Relevance
Nucleus	DNA synthesis, repair, replication	BrdU incorporation (DNA synthesis) γH2AX (double strand DNA breaks).	Ataxia telangiectasia, Nijmegen breakage syndrome, Werner syndrome, Bloom Syndrome, Fanconi anemia, xeroderma pigmentosum, Cockayne syndrome, trichothiodystrophy.	BrdU and EU incorporation measurements do not require morphologic assessment. γH2AX staining requires visualization (distinction of foci in the nucleus). Increased yH2AX staining is associated with disease. However, DNA damage first needs to be induced with DNA damaging agents or irradiation and the sensitivity to these agents differs per disease (radiation, chemotherapeutics, etc.)
	RNA synthesis, processing and transport	5-Ethynyl Uridine incorporation (RNA synthesis)	Mutations in RNA polymerase genes, the Mediator complex, the spliceosome, RNA editing, RNA export, etc.	
Endoplasmic Reticulum (ER)	Synthesis of lipids and proteins	ER Stress: ATF6 antibody translocation (ER stress) ER morphology: Calreticulin antibody (morphology) Calnexin antibody (morphology)	Congenital disorders of glycosylation, neurodegenerative diseases, diabetes and cancer.	ATF6 translocation reflects ER stress, is associated with disease and visualization of morphology is required to measure functionality.
				ER morphology reflects ER function, is associated with disease and requires morphologic assessment.
Golgi	Modification, sorting, and packaging of proteins and lipids for secretion or delivery to organelles.	GM130 antibody (morphology) AP1G1 antibody (protein sorting in the golgi)	Congenital disorder of glycosylation (CDG), Menkes disease, Wilsons disease, neurodegenerative diseases.	Golgi fragmentation or swelling reflect golgi dysfunction, altered golgi morphology is observed in many different diseases.

Mitochondria	ATP synthesis through oxidative phosphorylation	NAO (mitochondrial mass), TMRM (membrane potential), MitoSox (ROS production)	Primary mitochondrial diseases, diseases associated with mitochondrial fission and/or fusion.	Mitochondrial mass and morphology are essential for mitochondrial function and involved in the pathophysiology of many diseases.
Lysosomes	Intracellular degradation	LAMP1 antibody, Lysotracker	Lysosomal storage disorders (Batten disease, Gaucher disease, Niemann Pick syndrome).	Enhanced lysosomal size correlates with lysosomal storage disorder disease pathophysiology and disease severity.
Autophagosomes	Degradation and recycling of cellular components.	LC3B or p62 antibodies.	Vici syndrome, X-linked myopathy with excessive autophagy (VMA21), Niemann Pick type C1.	LC3B visualization is essential to distinguish autophagosomes from background, and to distinguish micro- from macro autophagy. Autophagy is involved in the pathophysiology of many diseases.
Endosomes	Sorting of endocytosed material.	EEA1antibody (early endosomes), RAB5a, RAB4A, RAB11, LAMP1 antibodies (late endosomes)	Niemann Pick syndrome, neurodegenerative diseases, TRAPPC mutations.	Enlarged size of endosomal compartment is associated with pathophysiology of several diseases.
The cytoskeleton	Maintains cellular shape and organization, provides mechanical support that enables cells to carry out essential functions like division and movement.	Phalloidin	Actinopathies, Wiskott-Aldrich syndrome (WAS), PFIT syndrome,	Alterations in actin cytoskeletal morphology have been associated with disease. Visualization is required to study the actin cytoskeleton.
		α-tubulin antibody, SiR-tubulin, Tubulin Tracker.	Tubulinopathies	Microtubules can better be studied dynamically, not statically.
Peroxisome	Oxidative breakdown of toxic molecules	Catalase antibodies.	Peroxisome biogenesis disorders, Zellweger syndrome spectrum (PBD-ZSS)	Catalase scattering can be used as a marker for peroxisomal disorders. Visualization is required.
Cellular signaling pathways	Control of cellular processes in relation to internal or external triggers.	mTOR, NF-κβ, JAK-STAT, NLPR3, MAPK, HIF1 antibodies.	Many genetic diseases are caused by defective intracellular signaling	If the signaling pathway involves (nuclear) translocation, assessment of morphology is essential. From all cellular signaling pathways, NF-κβ was chosen as a proof of principle. In theory, any kind of signaling pathway can be measured.

Table S1: Overview of assays included in the IFC platform for our pilot study.

Table S2: Validation of Imaging Flow Cytometry Features

Assay	Feature	Mask	Compound		Patient Control	
			Log2 foldchange	P-value	Log2 foldchange	P-value
Mitochondrial Mass	NAO Intensity	NA	-1.44	$7.475x10^{-06}$ ***	-0.63	0.02*
Membrane Potential	TMRM Intensity	NA	-1.01	$< 2.2x10^{-16}$***	-1.04	$9.81\ x10^{6}$***
Autophagy	LC3 spot Count	Spot Bright Threshold: 10 Minimal size:1 pixel Maximum size: 5 pixels	1.48	$< 2.2x10^{-16}$***	1.02	$< 2.2x10^{-16}$***
Lysosomal Accumulation	LAMP1 Area	Brightfield Adaptive Erode 70%	*NA*	*NA*	2.83	$< 2.2x10^{-16}$***
ER Stress	Similarity ATF6 - Score nucleus	Morphology Nucleus	3.15	$< 2.2x10^{-16}$***	1.17	$3.33x10^{6}$***
Golgi Fragmentation	% Fragmented	Threshold Golgi 70%	0.67	0.004*	3.06	0.003*
NF-κβ Translocation	Similarity Score p65 – nucleus.	Morphology Nucleus	2.00	$< 2.2x10^{-16}$***	NA	NA

Table S2 Overview of the features used to quantify aberrancies on assays and their validation. All assays and features were validated with a compound known to cause aberrancies in the pathway of interest ('Compound') and in patient cells ('Patient Control'). For each feature, the median value per patient or healthy control was calculated. The medians were compared between the patients serving as positive controls and all healthy controls (N=3 for all assays, except for the mitochondrial assay) using fold change and converted to log2 values. If positive patient controls groups consisted of two patients (CLN3, mitochondrial disease), the mean log2 foldchange was taken. The p-value was calculated using non-linear mixed model analysis and ANOVA. A significant p-value and log2 foldchange >1 or <-1 indicates the assay of interest is sensitive enough to pick up biological differences (log2foldchange >2).

Table S3: Clustering Accuracy with the inclusion of different numbers of healthy controls

Number of Healthy Controls	Number of Possible combinations	Clustering Accuracy
3	55	66%
4	69	60%
5	55	66%
6	27	68%
7	8	87.5%
8	1	100%

Table S3: To assesses how many healthy controls are needed to perform effective clustering, we attempted to separate patients from healthy controls using different numbers of healthy individuals. The first column shows the number of healthy control lines that were included to perform clustering. Since we had eight different healthy controls, there was a wealth of possible combinations of healthy controls that could be made, which is shown in the second column. The third column reflects the percentage of clustering attempts where the healthy controls were clustered separately from all patients and together as a group – which was considered correct clustering. Similar positive controls, clustering parameters and tools were used as in Figure 2D to perform clustering.

Figure S1: Gating strategy and masks used.

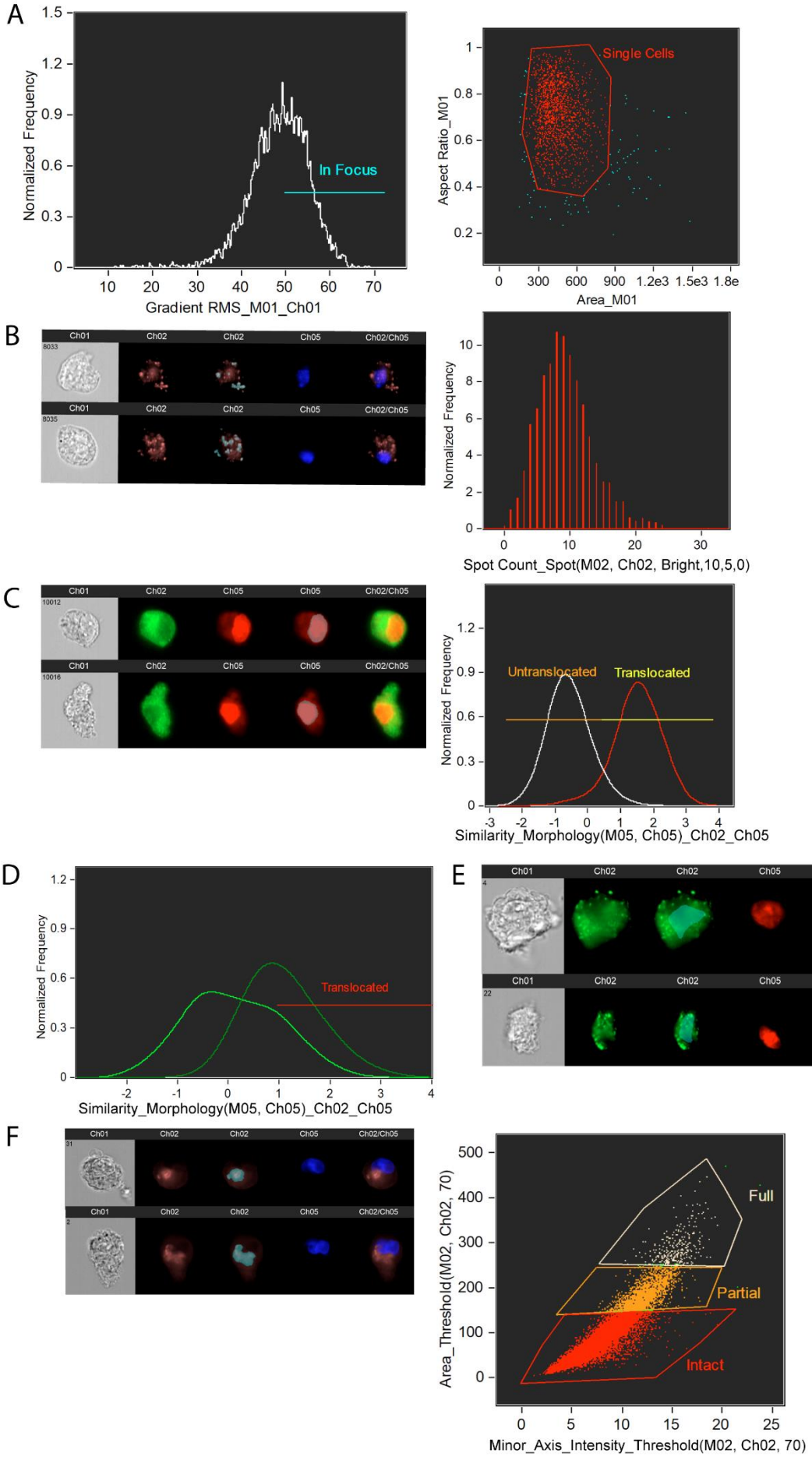
A
Normalized Frequency
In Focus
Gradient RMS_M01_Ch01
Single Cells
Aspect Ratio_M01
Area_M01
B
Ch01
Ch02
Ch05
Ch02/Ch05
Normalized Frequency
Spot Count_Spot(M02, Ch02, Bright,10,5,0)
C
Untranslocated
Translocated
Similarity_Morphology(M05, Ch05)_Ch02_Ch05
D
Translocated
Similarity_Morphology(M05, Ch05)_Ch02_Ch05
E
F
Full
Partial
Intact
Area_Threshold(M02, Ch02, 70)
Minor_Axis_Intensity_Threshold(M02, Ch02, 70)

Figure S1: Gating strategy and masks used.
(A) Showing the gating strategy used for all experiments. In Inspire, cells with nuclear intensity >$1x10^5$ were included for downstream analysis. In IDEAS, cells in focus were gated using the Gradient_RMS feature of the brightfield channel (Channel 1). Next, doublets were excluded by using the Area and Aspect Ratio of the brightfield image.
(B) Shows the specific gating for the autophagy assay. To count the number of autophagosomes, a Spot mask was created. On the left, the spot mask is shown as overlay (blue) over the LC3 staining (Channel 2, Ch02, light red). The nuclear staining (Channel 5, Ch05) is shown in blue. The graph on the right shows the Spot Count feature, which was combined with the spot mask, to quantify the number of autophagosomes.
(C) Shows the specific gating for the NF-κβ translocation assay. To measure the amount of p65 in the nucleus, a nuclear mask was created (Morphology_M05). The mask is shown as overlay (blue) over the nuclear staining (Channel 5, Ch05, red). In green, the p65 staining is shown (Channel 2, Ch02). The graph on the right shows the gating strategy to gate for p65 nuclear translocated and non-translocated cells. The pixel overlap between the p65 staining and the nuclear staining within the Morphology_M05 mask were used to quantify translocation (Using the feature Similarity_Morphology(M05, Ch05), Ch02_Ch05).
(D) Showing the gating strategy for the ER stress staining (ATF6 nuclear translocation). A similar strategy as for p65 translocation was used to quantify ER stress (the Morphology_M05 mask and Similarity_Morphology(M05, Ch05), Ch02_Ch05 feature).
(E) Shows the gating strategy for the LAMP1 staining. To measure the amount of lysosomes, the Adaptive Erode mask based on the brightfield image was used. In blue, the Adaptive_Erode_60 Mask of channel 1 is shown. To measure lysosomal accumulation within the entire cell, the Internalization of the LAMP1 staining within the Adaptive_Erode_60 mask was quantified.
(F) To quantify golgi fragmentation, first, a 70% threshold mask of the golgi staining (Channel 2, Ch02) was created. The 70% Threshold mask is shown in blue. The Golgi/GM130 staining is shown in light red. In blue, the nuclear staining is shown (Channel 5, Ch05). The graph shows the gating strategy to gate for cells with intact-, partially fragmented- or a fully fragmented golgi system.

Figure S2: Effect of fibroblast confluency on IFC assays.

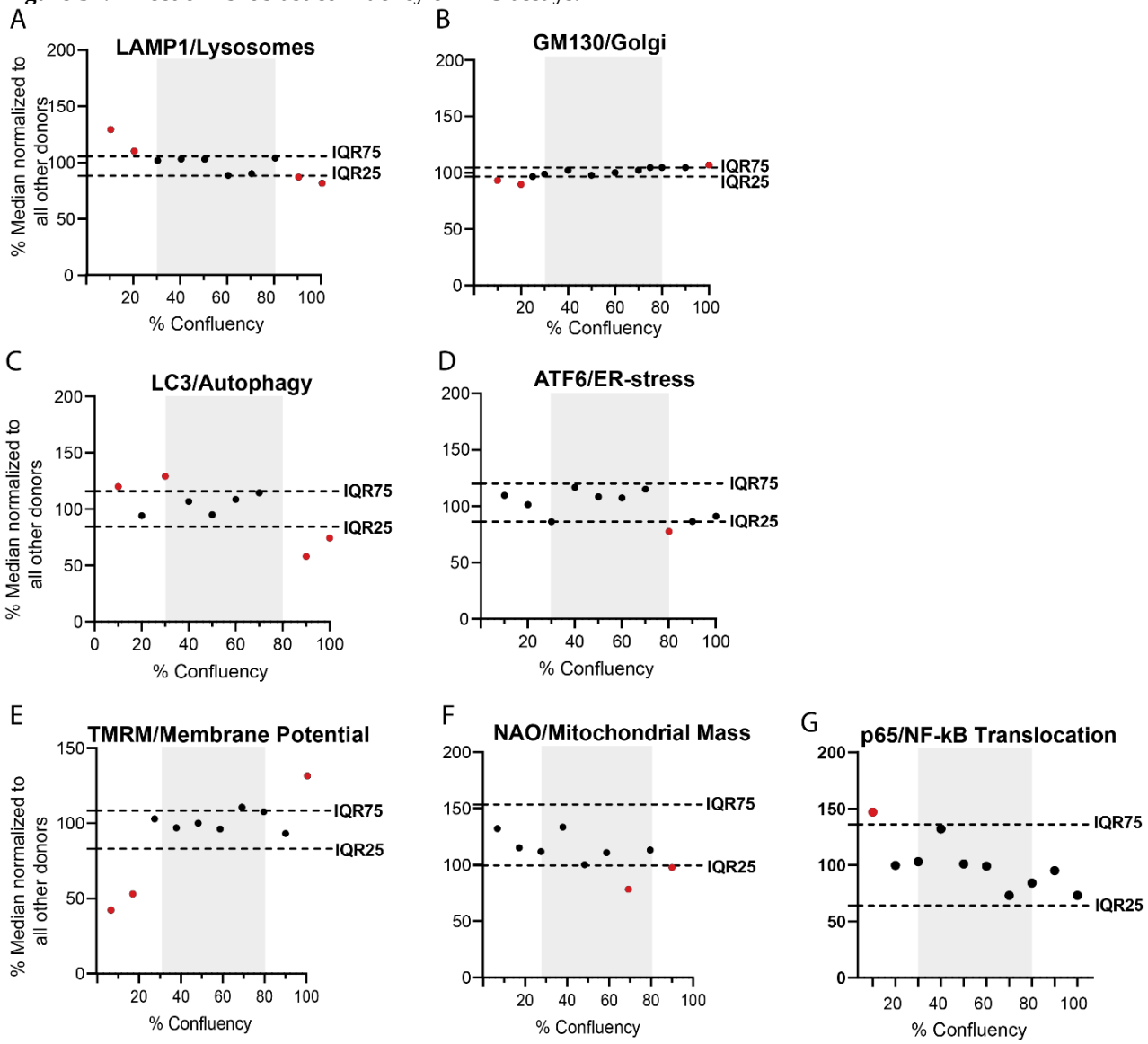

Figure S2: Effect of fibroblast confluency on IFC assays. Cells were plated to reach the desired confluence on the day of the assay. Actual confluence was quantified on the day of the assay using ImageJ, calculating the fibroblast-covering surface in relation to the entire area. These percentages are shown on the X-axis. The median feature value for each confluency percentage was divided by all other medians and converted to a percentage, shown on the y-axis. (A) Showing the effect of fibroblast confluency on the LAMP1 assay. (B) Showing the effect of confluency on the Golgi assay. (C) Showing the effect of confluency on the autophagy assay. The 80% condition is missing. (D) Showing the effect of confluency on the ER stress assay. (E) Showing the effect of confluency on the membrane potential assay. To calculate the percentages for this graph, each confluency percentage was directly compared to 50% and converted to a percentage (10% to 50%, 20% to 50%, etc.). Therefore, the IQR values are not centered around zero. (F) Showing the effect of confluency on the mitochondrial mass assay. To calculate the percentages for this graph, each confluency percentage was directly compared to 50% and converted to a percentage (10% to 50%, 20% to 50%, etc.). Therefore, the IQR values are not centered around zero.

Figure S3: Effect of fibroblast passage number on IFC assays.

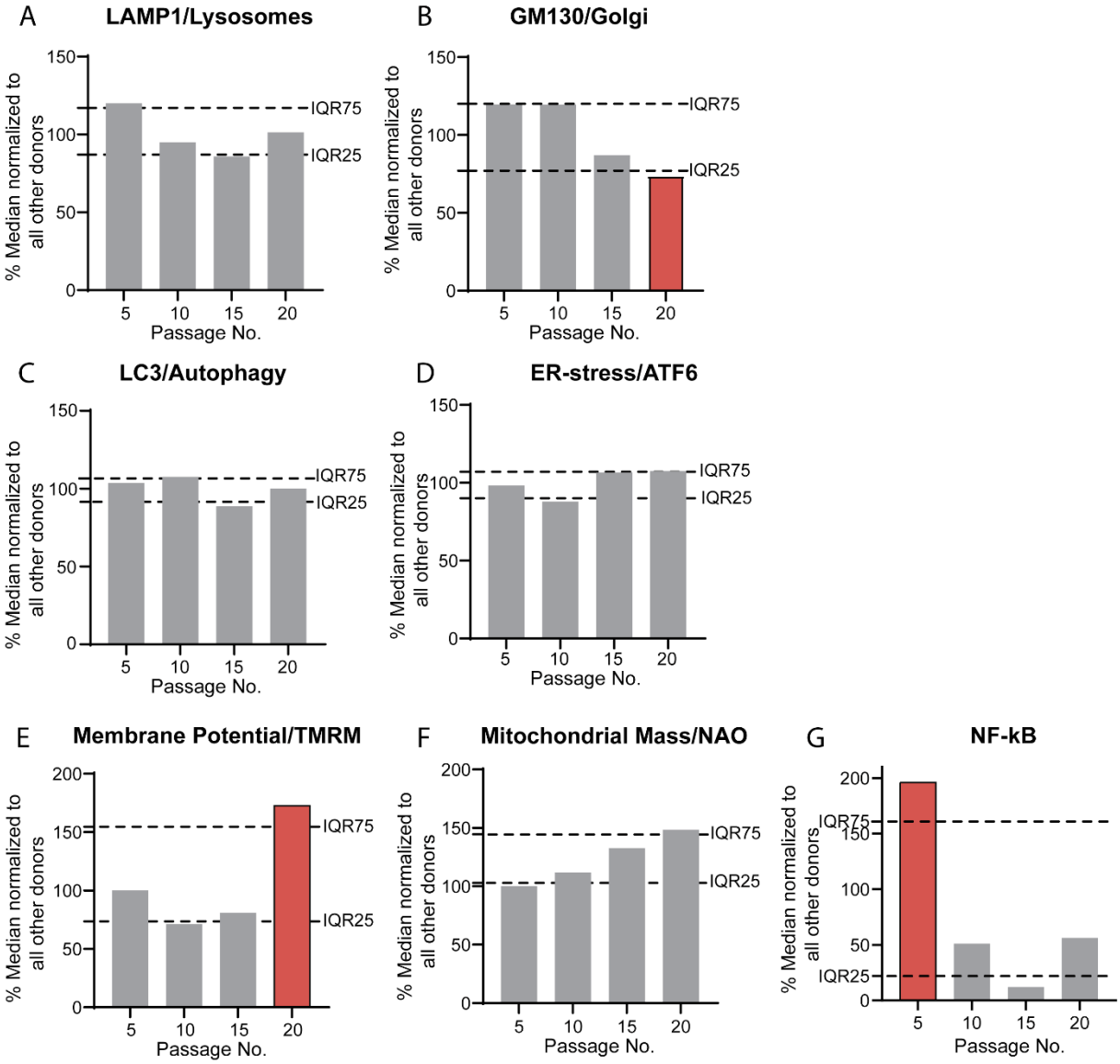

Figure S3: **Effect of fibroblast passage number on IFC assays.** For each individual analysis, the median feature value was divided by the median values of other replicates analyzed in the same experiment and converted to percentages. These percentages are shown on the Y-axis. The X-axis shows the fibroblast passage number. (A) Showing the effect of passage number on the LAMP1 assay. (B) Showing the effect of passage number on the golgi assay. (C) Showing the effect of passage number on the autophagy assay. (D) Showing the effect of passage number on the ER stress assay. (E) Showing the effect of passage number on the membrane potential assay. To calculate the percentages for this graph specifically, instead of comparing each value to all other values, each passage number was only compared to one other passage number and converted to a percentage (p5 to p10, p5 to p15, p5 to p20 etc). Therefore, the IQR values are not centered around zero. (F) Showing the effect of passage number on the membrane potential assay. To calculate the percentages for this graph, each passage number was directly compared to another passage number and converted to a percentage (p5 to p10, p5 to p15, p5 to p20 etc). Therefore, the IQR values are not centered around zero. (G) Showing the effect of passage number on NF-κβ translocation. NF-κβ translocation decreased significantly with advancing passage number, hence explaining the high level of translocation at p5.

Table S4: Assessment of pathogenicity of VUSes in well-known disease genes.

Donor	Gene	In-silico predictions (MutationTaster)	In-silico predictions (CADD score)	Functional Assays	ACMG
CLN33	*CLN3* Homozygous 1kb deletion in exon 6	NA	NA	Increased vacuoles in lymphocytes and increased % lymphocytes with vacuolization **(Figure S4)**	PVS1, **PS3**, Pathogenic
CLN34	*CLN3* Homozygous 1kb deletion in exon 6	NA	NA	Increased vacuoles in lymphocytes and increased % lymphocytes with vacuolization **(Figure S4)**	PVS1, **PS3**, Pathogenic
240	*TAZ* De Novo variant	Disease Causing	29.1	Severely increased MLCL/CL ratio **(Figure S4)**	PM6, PP2, PP3, PP4, PP5, **PS3** Pathogenic
111	*ACAD9* Homozygous missense variant	Polymorphism	20.5	Literature: 30% reduction of ACAD9 activity in protein extracts[1]	PP5, PP4, **PS3** Likely pathogenic
249	*DLP1* De Novo variant	Disease Causing, splice site changes	25.1	Mildly aberrant peroxisomal staining (beads on a string). Peroxisomal fission defect. Mildly aberrant mitochondrial staining: elongated mitochondria.	PS2, PP4, **PM1**, PP5, PM2 Likely Pathogenic
253	*DLP1* De Novo variant	Disease Causing, splice site changes	22.6	No peroxisomal aberrancies. Mildly aberrant mitochondrial staining: elongated mitochondria.	PM2, PP3, PS2**.** PS1. VUS
250	*EPG5* Homozygous missense variant	Disease Causing, splice site changes	25.5	No differences observed with p62/LC3 western blot	PS2, PP4, PM2, VUS

Figure S4: Diagnostic assays performed in individuals with VUS

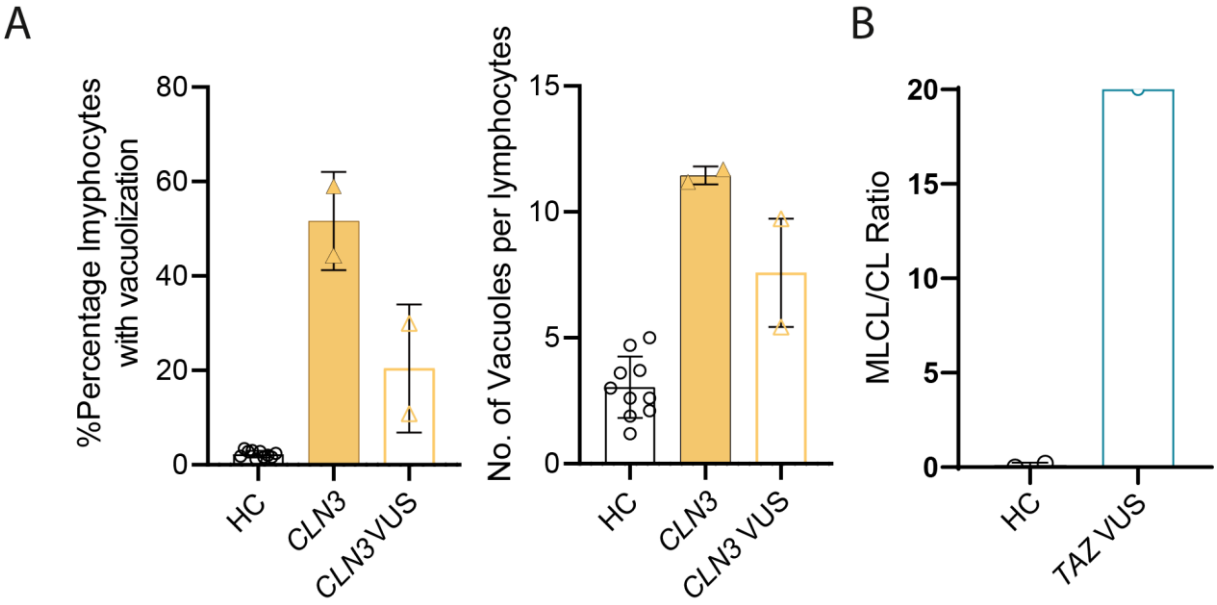

Figure S4: (A) Bar graphs showing the mean number of vacuoles per lymphocyte as well as the number of lymphocytes with vacuole ±SD. Both measures are the current gold standard to establish diagnosis of Batten disease. *CLN3* refers to the two patients with pathogenic variants, while *CLN3* VUS refers to the two individuals with VUSes in *CLN3*. The increased values in the individuals with *CLN3* VUSes indicate pathogenicity of variants.
(B) Bar graph showing the monolysocardiolipin:cardiolipin (MCLC:CL) ratio for the individual with a VUS in *TAZ*.

Table S5: Assessment of pathogenicity of VUSes

Donor	Gene	ACMG	In-silico predictions (MutationTaster)	In-silico predictions (CADD score)
143	*CSDE1* De Novo missense variant	PM2, PS2, PP3 VUS	Disease Causing	28.6
	ZFYVE16 De Novo missense variant	PS2, PP3 VUS	Disease Causing	21.1
140	*LIMK1* De Novo missense variant	PS2, PM2, PP3 VUS	Disease Causing	26.9
093	*LIMK1* De Novo missense variant	PS2, PP3 VUS	Polymorphism	13.3
225	No VUSes identified			
227	*BRWD3* Hemizygous De Novo variant	PS2, PM2, PP3 VUS	Disease Causing	23.5
	PDE3B Homozygous deletion	PM4, PS2, PP3 VUS	Disease Causing, frameshift	NA
228	*MMS19* De Novo missense variant	PM2, PS2, PP3 VUS	Disease Causing	31
211	*DLGAP2* De Novo duplication	PP3, PS2, PM4 VUS	Disease Causing, frameshift	NA

	TNKS De Novo missense variant	PP3, PM2 VUS	Disease Causing, splice site changes	21
106	*RAD54L2* De Novo missense variant	PP3, PS2, PM2 VUS	Disease Causing	25.7
226	*PDE4DIP* Compound Heterozygous missense variant	BP4, VUS	Polymorphism, Polymorphism	14.41, 1.9
	MEIOC De Novo missense variant	PM2, PS2, PP3 VUS	Disease Causing, splice site changes	23.4
202	*SLC4A2* De Novo missense variant	PS2, PP3 VUS	Disease Causing, splice site changes	28.1
217	*EIF4ENIF1* De Novo missense variant	PS2, PP3, PM2 VUS	Disease Causing	31

Figure S5: Assessment of batch effects with the implementation of 1800 IFC features.

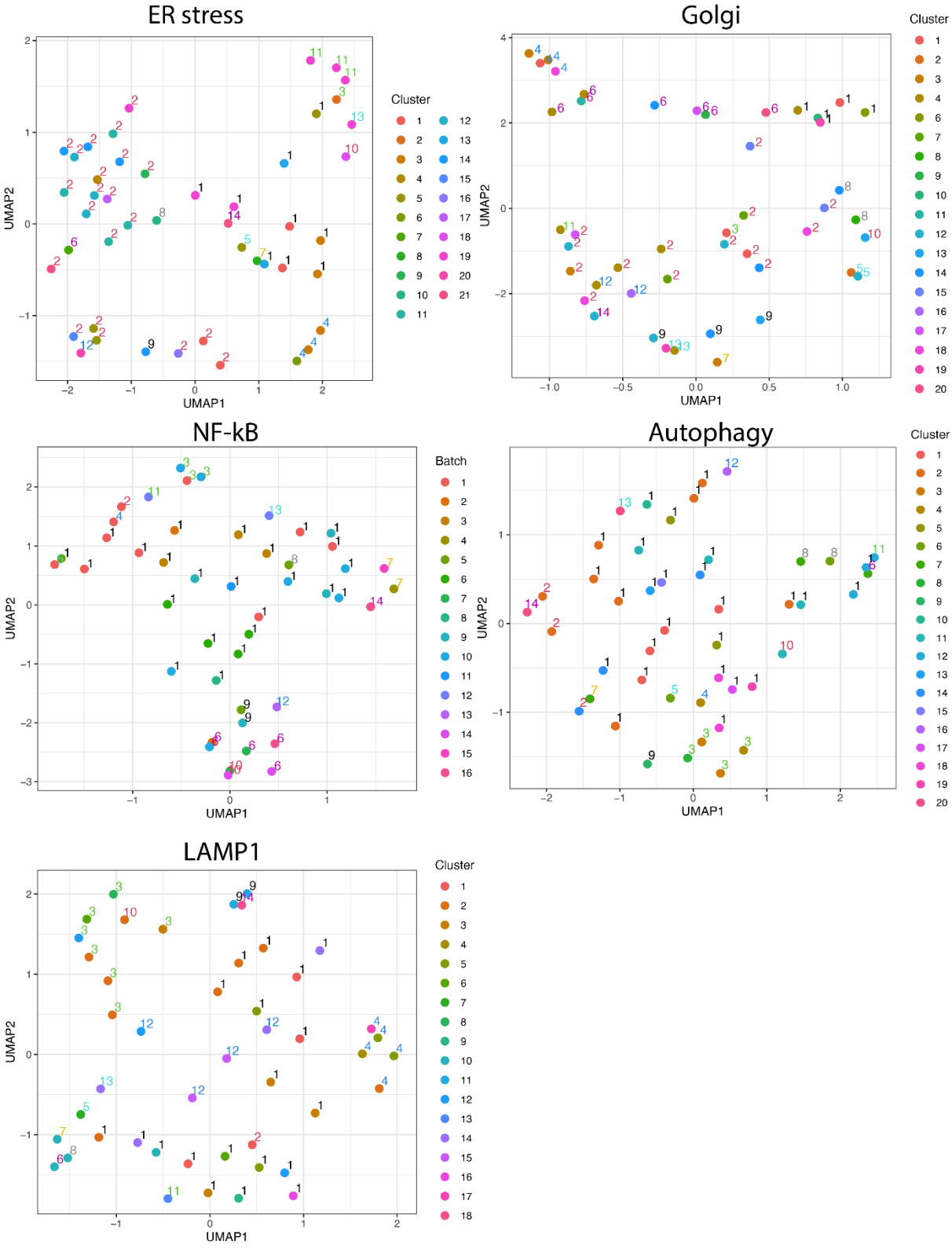

Figure S5: To assess batch effects, average linkage clustering based on Manhattan distance was used. UMAP was used for visualization. Batch effects were considered if donors analyzed within one single experiment clustered together. The experiment numbers /batch numbers are shown as actual numbers next to the colored dots. The color of the dot indicates the outcome of the Manhattan clustering. The number of clusters was determined using elbow plots. As can be seen, the batch numbers do not correlate with cluster numbers in any of

the assays, indicating the biological variation rather than batch effect contribute to differences between donors. Batch effects were assessed separately for (A) ER stress, (B) Golgi, (C) NF-κβ translocation, (D) Autophagy, (E) LAMP1.

1. Schiff M, Haberberger B, Xia C, et al. Complex I assembly function and fatty acid oxidation enzyme activity of ACAD9 both contribute to disease severity in ACAD9 deficiency. *Hum Mol Genet*. 2014;24(11):3238-3247. doi:10.1093/hmg/ddv074